ELSEVIER

Journal of Hydrology 191 (1997) 179–207

Journal of Hydrology

Physics of the spatially averaged snowmelt process

Federico E. Horne*, M. Levent Kavvas

Department of Civil and Environmental Engineering, University of California, Davis, CA 95616, USA

Received 1 July 1995; revised 24 January 1996; accepted 29 February 1996

Abstract

It has been recognized that the snowmelt models developed in the past do not fully meet current prediction requirements. Part of the reason is that they do not account for the spatial variation in the dynamics of the spatially heterogeneous snowmelt process. Most of the current physics-based distributed snowmelt models utilize point-location-scale conservation equations which do not represent the spatially varying snowmelt dynamics over a grid area that surrounds a computational node. In this study, to account for the spatial heterogeneity of the snowmelt dynamics, areally averaged mass and energy conservation equations for the snowmelt process are developed. As a first step, energy and mass conservation equations that govern the snowmelt dynamics at a point location are averaged over the snowpack depth, resulting in depth averaged equations (DAE). In this averaging, it is assumed that the snowpack has two layers. Then, the point location DAE are averaged over the snowcover area. To develop the areally averaged equations of the snowmelt physics, we make the fundamental assumption that snowmelt process is spatially ergodic. The snow temperature and the snow density are considered as the stochastic variables. The areally averaged snowmelt equations are obtained in terms of their corresponding ensemble averages. Only the first two moments are considered. A numerical solution scheme (Runge–Kutta) is then applied to solve the resulting system of ordinary differential equations. This equation system is solved for the areal mean and areal variance of snow temperature and of snow density, for the areal mean of snowmelt, and for the areal covariance of snow temperature and snow density. The developed model is tested using Scott Valley (Siskiyou County, California) snowmelt and meteorological data. The performance of the model in simulating the observed areally averaged snowmelt is satisfactory.

* Corresponding author at: Facultad de Ciencias Agrarias, Universidad Nacional del Comahue, 8300 Neuquen, Argentina.

PII S0022-1694(96)03063-6

1. Introduction

Snow constitutes an important part of the water resources in many countries. Because it accumulates during the winter and melts in the spring, it is a strategic resource for irrigated agriculture. Therefore, it is critical to have accurate snowmelt runoff estimates. Snowmelt runoff estimation is needed also for flood warning, reservoir management, and hydroelectric power planning.

Spatial representation of the snowmelt process is a research problem yet to be solved. Although the physics of the snow cover at a point scale is well understood (Anderson, 1976; Dunne et al., 1976; Male and Gray, 1981; Morris, 1983; Kondo and Yamazaki, 1990), very few studies deal with spatially distributed snowmelt models.

Morris (1985) pointed out that many basin-scale snow models utilize point-location-scale conservation equations. However, such an equation system conserves the mass and energy only at a point location. Let one place a computational grid network with a spatial resolution of, say 100 m, over a watershed area to compute the snowmelt process. Then if one utilizes point-location-scale conservation equations for the computation of snowmelt at each nodal point of this grid network, one makes the fundamental assumption that the snowmelt process is spatially homogeneous over the 100 m × 100 m area which surrounds each computational node. However, the snowmelt over a 100 m × 100 m area is spatially heterogeneous. If one moves a few meters from the location of the computational node, the snowmelt rate could be very different from that at the node. Therefore, under the spatial heterogeneity of the snowmelt dynamics, what is computed by point-location-scale conservation equations at a computational node represents only the snowmelt dynamics at that point location, and may not necessarily represent the spatially heterogeneous melt rates over the grid area that surrounds that node. To better approximate the spatial homogeneity of snowmelt over each area, surrounding each node, one may take a much finer spatial resolution for the computational grid network (less than 10 m). However, in that case the hydrologist would end up with the great difficulty of estimating the point-location-scale parameters over several hundred thousand computational nodal locations over the snowmelt computation area. Such an approach would require a very large amount of spatially distributed data. It would also require the computation of the snowmelt process over several hundred thousand nodes at each time increment.

One approach to alleviate these difficulties in the application of point-location-scale conservation equations to the snowmelt computation over a large area is the development of areally averaged conservation equations for the snowmelt physics. As the model, evaluated at each node of a computational grid, needs to be representative of the snowmelt dynamics taking place over the grid area which surrounds a computational node, it is plausible to integrate the mass and energy conservation equations of snowmelt over such a grid area, and use these equations at the node surrounded by the area. As areal-averaging amounts to integration of snowmelt over an area and dividing the integral by the size of the area, such areally averaged snowmelt conservation equations would then represent the areally averaged snowmelt process over the area which surrounds each computational node. In this way, the scale of the conservation equations will be consistent with the scale of each grid area. Furthermore, as will be shown in the following developments of such an areally averaged model, the emerging parameters of such a model become

areally averaged quantities themselves, being consistent with the size of the grid area which is represented at a computational node. With this approach, one could take as large a grid area as possible as long as the ergodicity of the snowmelt process is satisfied over such a grid area. In this manner, one could realize significant savings both in parameter estimation work and in computation of the snowmelt over an area.

One may pose the question of how an areally averaged snowmelt model can describe the spatial variation of snowmelt over any computational grid area. As will be shown in the following model developments, the areal variation of the snowmelt process is described by the areal variance and areal covariance equations of the snowmelt dynamics. Therefore, the areally averaged conservation equations for the snowmelt process consist of not only the areal mean but also the areal variance and areal covariance of the state variables of the snowmelt process.

2. Depth averaging of the governing equations

2.1. Point equations

Snow is a three-phase system composed of a mixture of water (gas, liquid and ice) and air in proportions that depend on the energy balance. Source energy is provided internally by latent heat owing to phase change and externally by heat exchange with the atmosphere and by solar radiation. Energy is stored as heat in each phase and is subject to advection within the snowpack.

The point-scale equations for the conservation of mass and energy (over differential control volumes) were formulated by Morris (1982, 1983). Subscripts i, w and v are used to denote ice, water and vapor. The point-scale mass continuity equation for the component k is (Morris, 1983)

$$\frac{\partial}{\partial t}(\rho_k\theta_k)+\frac{\partial}{\partial z}(\rho_k\theta_k v_k)=\sum_j M_{kj} \tag{1}$$

The equation for the conservation of energy is (Morris, 1982)

$$\sum_k\left[\rho_k\theta_k(C_p)_k\frac{\partial T}{\partial t}+\rho_k\theta_k v_k(C_p)_k\frac{\partial T}{\partial t}\right]= \frac{\partial}{\partial z}\left(\kappa\frac{\partial T}{\partial z}\right)+M_{\mathrm{wv}}L_{\mathrm{wv}}+M_{\mathrm{iw}}L_{\mathrm{iw}}+M_{\mathrm{iv}}L_{\mathrm{iv}}+\frac{\partial Q_{\mathrm{n}}}{\partial z} \tag{2}$$

where ρ_k is density of component k (g cm^{-3}); θ_k is volume per unit volume of snow for component k; v_k is velocity in the vertical direction for component k (cm h^{-1}); t is time (h); M_{kj} is mass of component k produced per unit volume per unit time by a phase change from component j (g cm^{-3} h^{-1}); $(C_p)_k$ is specific heat at constant pressure of component k (cal g^{-1} °C^{-1}); T is temperature of the mixture (°C); κ is thermal conductivity (cal h^{-1} cm^{-1} °C^{-1}); Q_{n} is net radiation energy (cal cm^{-2}); L_{kj} is latent heat released by transformation M_{kj} (cal g^{-1}). (Every term in the mass equation, Eq. (1), is given in g cm^{-3} h^{-1}. In the energy equation, Eq. (2), terms are in cal cm^3 h^{-1}.)

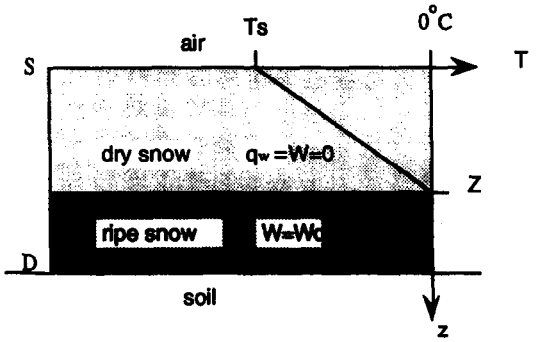

Fig. 1. Snowpack model.

Several assumptions are made often to simplify these equations. It is usually assumed that the ice matrix is at rest, i.e. $v_i = 0$. Therefore, melting or snowfall do not involve a movement of the ice grains in the snowpack. Additionally, the heat capacity of the gaseous phase is very small compared with those of ice and water and may be ignored. Also, the pressure of the moist air can be considered constant. With these assumptions, the Eq. (2) now becomes

$$[\rho_i\theta_i(C_p)_i+\rho_w\theta_w(C_p)_w]\frac{\partial T}{\partial t}+\rho_w\theta_w(C_p)_w]\frac{\partial T}{\partial z}= \frac{\partial}{\partial z}(\kappa\frac{\partial T}{\partial z})+M_{wv}L_{wv}+M_{iw}L_{iw}+M_{iv}L_{iv}+\frac{\partial Q_n}{\partial z} \tag{3}$$

To average the energy equation over the snow depth, an active layer model is adopted. It is assumed that the temperature of the snow varies linearly with the depth until the freezing level Z is reached (Kondo and Yamazaki, 1990). Below that, the temperature remains constant at 0°C. The freezing depth layer will move vertically responding to the energy balance. It is assumed that the water content W of the snowpack is zero above Z and that it takes a constant value W_0 below Z as shown in Fig. 1. The linear relationship between T and Z allows us to write the average snow depth temperature of the snowpack $\bar{T}$, *as* $\bar{T}=\frac{1}{2}T_s$.

A constitutive relationship can be expressed by the following equation of state of the snowpack:

$$W=0 \text{ for } T<0°C$$

$$W=W_0 \text{ for } T=0°C \tag{4}$$

where W_0 is the gravitational water content of the snow, defined as the ratio of mass of liquid water to the mass of wet snow. As θ_w is a volume variable, one can take

$$\theta_w\rho_w=W_0\rho_s \tag{5}$$

If the air mass in the snow is ignored, it can be assumed for dry snow that the mass of ice is equal to the mass of snow;

$$\theta_i\rho_i=\rho_s \tag{6}$$

A positive energy balance will result in a shallower freezing depth Z (see Fig. 1) by which fusion heat will be used to produce water from a dry snow. When the whole snow profile D reaches a saturation state ($z = 0$ and $T = 0°C$) any additional heat surplus M will yield snowmelt contributing to the runoff. The relationship between the snowmelt energy M and the water production by the snowpack, M_r, can be written as

$$M_r = \frac{M}{[L_f \rho_w (1 - W_0)]} \quad (\mathrm{cm_w^3\ cm_s^{-3}\ h^{-1}}) \tag{7}$$

where $(1 - W_0)$ is defined by DeVries and Franke (1988) as the thermal quality of the snow. It represents the heat necessary to produce a given amount of melt water from the existing snow, as the same quantity of melt from pure ice.

2.2. *Integration of energy equation through the depth of snowpack*

Conservation equations averaged over the snow depth usually deal only with the mean properties of the snowpack and do not consider spatial variability occurring within the pack. However, by considering two layers, the main properties of the snow may be captured.

Integration of the point-scale energy equation, Eq. (3), throughout the depth of the snowpack is performed in two steps: (1) from $z=0$ (surface) to $z = Z(t)$; (2) from $z=Z(t)$ to $z = D$, the snowpack depth. Given that one of the integration limits is changing with time, the Liebnitz rule was used in the integration. In Eq. (3) $(C_p)_i$ and the mean vertical density $\bar{\rho}_s$ for the snow cover profile are considered constant. The energy fluxes (negative downward) at the top of the pack are given by

$$-(sw_0 + I_{in} - I_{out} + H - L_v E_v + Q_p)$$

where sw_0 is the incoming shortwave solar radiation, $I_{in} - I_{out}$ is the incident minus reflected longwave radiation, H is the sensible heat exchange with the atmosphere by turbulent transfer, E_v is the evaporation, L_v is the latent heat of vaporization, and Q_p is the heat convected to the pack by precipitation. At the bottom of the pack the energy fluxes are given by

$$-(sw_D + M + Q_g)$$

where M has already been defined as the energy required to produce snowmelt, Q_g is the heat exchange with the soil (negative downward) and sw_D is the attenuated shortwave radiation at the bottom. Applying the assumptions made for the two-layer model of Fig. 1 and neglecting the convection of energy owing to variations in the snowpack height as well as the latent heat of sublimation–solidification by assuming $M_{iv}L_{iv} = 0$, the vertical integration of the energy equation, Eq. (3), leads to the following depth-averaged energy equation for the snowpack:

$$\bar{\rho}_s (C_p)_i Z \frac{d\bar{T}}{dt} + \bar{\rho}_s [(C_p)_i \bar{T} - L_f W_0] \frac{dZ}{dt} = sw_0 - sw_D + I_{in} - I_{out} + H - L_v E_v - M + Q_p - Q_g \tag{8}$$

It is difficult to estimate the heat Q_p convected by rain. Kondo and Yamazaki (1990)

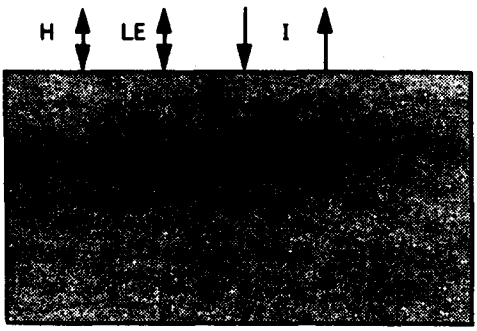

Fig. 2. Energy exchanged at the snow surface.

considered that it is small enough to be ignored, i.e. 10 mm of rain at 10°C can melt only 1 mm day^{-1} in water equivalent. The heat exchanged with the ground is even less except in early winter (Kojima and Motoyama, 1985). Experimental results presented by Kuz'min (1961) show that the calculated heat exchange with the ground never exceeds 10 cal cm^{-2} day^{-1}. Morris (1985) also indicated that the heat exchange with the ground by conduction is very small compared with the energy fluxes at the upper boundary. The use of a constant value of 0–10 cal cm^{-2} day^{-1} was suggested. Similar conclusions were reached by Smith (1974). Neglecting the rain and ground heat exchanges, Eq. (8) becomes

$$\bar{\rho}_s(C_p)_i Z\frac{d\bar{T}}{dt}+\bar{\rho}_s[(C_p)_i\bar{T}-L_f W_0]\frac{dZ}{dt}=sw+G_1-M \tag{9}$$

where sw is the net shortwave radiation component absorbed by the pack, and

$$G_1=I_{in}-I_{out}+H-L_v E_v$$

G_1 is the energy exchanged across the upper boundary, excluding the net incoming shortwave radiation. As will be described later, G_1 can be approximated by a linear function of the surface snow temperature.

The right-hand side of Eq. (9) includes the driving force terms that represent the energy exchanged by the snowpack. This energy may increase the temperature of the upper layer of the pack (first left-hand side term) and/or raise the freezing depth layer (second left-hand side term) by melting dry snow. The snowmelt energy M is taken as zero except when $\bar{T}=0$°C and $Z=0$. A relationship between T and Z can be obtained from the heat flow balance in the surface layer as shown in Fig. 2. If a heat balance is performed on an infinitesimally thin snow layer according to Fig. 2, one can take (Kondo and Yamazaki, 1990)

$$\lambda_e\frac{dT}{dz}=G_1 \tag{10}$$

It should be noted that the shortwave radiation is not included. In fact, sw is either transmitted or reflected in this 'skin' layer.

The effective thermal conductivity λ_e is used in place of the thermal conductivity, to allow for the thermal effect of the transport of water to be taken into account indirectly. This term captures most of the heat transferred owing to the vapor carried by a temperature

gradient. On the other hand, as it is virtually impossible to separate the effects of the conduction and diffusion processes, it is customary to express the measured value as an effective conductivity of the snowpack.

As the temperature gradient is assumed to be linear in the adopted snowpack model, the snow surface temperature T_s is expressed as $T_s = 2\bar{T}$ (Fig. 1). Therefore, Eq. (10) can be written in terms of $\bar{T}$ as

$$G_1 = \frac{2\lambda_e \bar{T}}{Z} \tag{11}$$

Although λ_e depends on the state of the crystalline structure of the snow, most of the experimental determination of λ_e has been correlated solely with snow density ρ_s. A quadratic relation of the form

$$\lambda_e = k_1 + k_2 \bar{\rho}_s^2 \tag{12}$$

can be adopted based on the experimental results obtained by several investigators (see e.g. Yen, 1962).

2.3. Density changes in the snowpack

As the changes in the density that are controlled by metamorphic processes are not fully understood, here only the changes owing to the compacting and temperature gradient processes are considered. These two processes have been quantified and validated in the last 40 years by Bader et al. (1939), Mellor (1964), Kojima (1967), Anderson (1976) and others.

The seasonal compacting of snow can be estimated by the expression presented by Yosida (1955):

$$\frac{1}{\rho_s}\frac{d_s}{dt} = \frac{w_s}{\eta} \tag{13}$$

where w_s is the weight of snow above the layer for which the density change is being computed, in water equivalent (cm), and η is the viscosity coefficient, a constant for a given temperature and snow density (cm h^{-1}). η can be calculated as the result of two different multiplicative effects, compacting and temperature changes: $\eta = \eta_c \eta_t$. Kojima (1967) obtained from experimental measurements an expression for η_c:

$$\eta_c = \eta_{c0} \exp(k_0 \rho_s) \tag{14}$$

where η_{c0} is the viscosity when ρ_s is reduced to zero (cm h^{-1}) and k_0 is a constant value in the range 15–38 (cm^3 g^{-1}).

Mellor (1975), on the basis of observations of natural snow in polar regions, developed an equation for the viscosity coefficient η_t. This expression included the temperature gradient effect:

$$\frac{\eta_t}{\eta_{t0}} = \exp\left[\frac{A}{R}\left(\frac{T_c - T}{T T_c}\right)\right] \tag{15}$$

where A is the activation energy of snow (10^4 cal mol^{-1}), R is the gas constant (2 cal mol^{-1} K^{-1}), T_c is the critical temperature (0°C), and η_{t0} is η_t at 0°C.

For the temperatures normally experienced in areas with seasonal snow cover, ($A/(RTT_c)$) may be about 0.08 K^{-1} according to Anderson (1976). Integration of Eq. (14) over the snow depth can be approximated by considering $\bar{\rho}_s$ as the density corresponding to the point located at $2D/3$, where D is the snowpack depth (Van der Heydt, 1991). Utilizing this approximation in Eq. (14) and substituting Eq. (14) and Eq. (15) into Eq. (13) yields

$$\frac{d\bar{\rho}_s}{dt} = \left(\frac{2}{3}D\right)\bar{\rho}_s^2\eta_0^{-1}\exp[-0.08(T_c-\bar{T})]\exp[-k_0\bar{\rho}_s] \tag{16}$$

where η_0 is the viscosity coefficient at 0°C and zero density. This expression has been also presented by Kutchment et al. (1983) and Motovilov (1986).

2.4. Simplified expression of the energy balance

The net longwave radiation captured by the snowpack can be estimated by the Stefan–Boltzmann Law applied to the incoming and reflected energy fluxes:

$$I_n = 0.92\times10^{-5}\sigma T_a^6 - \epsilon_s\sigma T_s^4$$

where ϵ_s is snow emissivity, σ is Stefan–Boltzman constant, and T_a and T_s are air and snow temperatures, respectively. The estimation by Swinbank (1963) for atmospheric emissivity ϵ_a was adopted here for the incoming longwave radiation. The emissivity of the snow, ϵ_s, takes values between 0.97 and 1.0. Applying the Taylor series, one can expand I_n around T_a to obtain

$$I_n = 0.92\times10^{-5}\sigma T_a^6 - \epsilon_s\sigma T_a^4 - 4\epsilon_s\sigma T_a^3(T_s-T_a) \tag{17}$$

Turbulent transfers of sensible and latent heat to the atmosphere can be estimated by applying the aerodynamic technique (Prandtl, 1932) for one observation height:

$$H = D_h U_z(T_a - T_s) \tag{18}$$

$$L_v E_v = D_e U_z[e_{(T_a)} - e_{(T_s)}] \tag{19}$$

where

$$D_h = \frac{C_p\rho\, k^2}{(\ln z_2/z_1)^2}\frac{K_h}{K_m} \text{ and } D_e = \frac{0.622L_v\,\rho\, k^2}{P(\ln z_2/z_1)^2}\frac{K_e}{K_m}$$

In Eq. (19), U_z is the wind speed and $e_{(T)}$, the vapor pressure at temperature T, is related to specific humidity q by $e_{(T)} = qP/0.622$, where P is the atmospheric pressure. D_h and D_e are bulk transfer coefficients for convected heat and for latent heat transfer, respectively. In the expressions for D_h and D_e, K_m, K_h and K_e are eddy diffusivities for momentum, sensible heat and latent heat transfers, respectively. Also, k is the von Kármán constant, and z_2 and z_1 are two reference elevations in the atmosphere where observations are made. Values for D_h and D_e have been reported by various investigators (e.g. Male and Gray, 1981). These values are obtained by measuring the air temperature, wind velocity and

humidity at a reference height, assuming logarithmic variation with elevation (Businger et al., 1971).

The latent heat transfer to the atmosphere, Eq. (19), can be expressed as a function of temperature and relative humidity. The saturated vapor pressure $e^*_{(T)}$ can be calculated as a function of temperature using the Clausius–Clapeyron equation:

$$e^*_{(T)} = 6984.5 + T[-188.9 + T(2.133 + T\{-1.289 \times 10^{-2} + T[4.39 \times 10^{-5} + T(-8.024 \times 10^{-8} + 6.137 \times 10^{-2} T)]\})] \tag{20}$$

On the snow surface, the vapor pressure is considered to be the pressure of saturation and is calculated using Eq. (20) with the temperature of snow at the surface. The air vapor pressure can also be written as a function of the air saturated vapor pressure if h, the relative humidity, and T_a, the air temperature, are known:

$$e_{(T_a)} = e^*_{(T_a)} h \tag{21}$$

Applying Eq. (20) to the snow surface and expanding around T_a, one obtains

$$e^*_{(T_s)} = e^*_{(T_a)} + \left[\frac{\partial e^*_{(T)}}{\partial T}\right]_{T_a} (T_s - T_a) \tag{22}$$

Substituting Eq. (21) and Eq. (22) in Eq. (19) yields

$$L_v E_v = -D_e U_z \{e^*_{(T_a)}(1-h) + \left[\frac{\partial e^*_{(T)}}{\partial T}\right]_{T_a} (T_s - T_a)\} \tag{23}$$

Eqs. (17), (18) and (23) are linear expressions of the snow temperature T_s. Therefore, the longwave radiation and turbulent transfer terms, denoted as G_1, can be simplified to the expression

$$I_n + H + L_v E_v = G_1 = A + BT_s \tag{24}$$

where

$$A = 3.80859 \times 10^9 \sigma + 8.37052 \times 10^7 T_a \sigma + 766531 T_a^2 \sigma + 3743.74 T_a^3 \sigma + 10.285 T_a^4 \sigma + 0.0150696 T_a^5 \sigma + 9.2 \times 10^{-6} T_a^6 \sigma - 5554571841.0 \epsilon_s \sigma + 447174 T_a^2 \epsilon_s \sigma + 2184.07 T_a^3 \epsilon_s \sigma + 3 T_a^4 \epsilon_s \sigma + 83.3938 D_e U_z + D_h T_a U_z + 0.0122117 D_e T_a^2 U_z + 0.000527205 D_e T_a^3 U_z + 0.00000906021 D_e T_a^4 U_z + 8.11362 \times 10^{-8} D_e T_a^5 U_z + 3.0685 \times 10^{-10} D_e T_a^6 U_z - 83.3938 D_e h U_z - 0.362288 D_e T_a h U_z + 0.0122117 D_e T_a^2 h U_z + 0.000263603 D_e T_a^3 h U_z + 3.02007 \times 10^{-6} D_e T_a^4 h U_z + 2.02841 \times 10^{-8} D_e T_a^5 h U_z + 6.137 \times 10^{-11} D_e T_a^6 h U_z$$

and

$$B = -162771336\epsilon_s\sigma - 1788696T_a\epsilon_s\sigma - 6552T_a^2\epsilon_s\sigma - 8T_a^3\epsilon_s\sigma + 0.724575D_eU_z - 2D_hU_z - 0.0488467D_eT_aU_z - 0.00158162D_eT_a^2U_z - 0.0000241606D_eT_a^3U_z - 2.02841\times10^{-7}D_eT_a^4U_z - 7.3644\times10^{-10}D_eT_a^5U_z$$

2.5. Integration of the mass balance equation through the snowpack

The point-scale conservation of mass equation, Eq. (1), is simplified assuming that the snow composition remains constant. The assumption is commonly made in lumped (in depth) models. Neglecting the mass exchanged between ice and vapor phases ($M_{iv} = 0$), Eq. (1) can be written as

$$\frac{\partial}{\partial t}(\bar{\rho}_i\theta_i) + \frac{\partial}{\partial z}(\bar{\rho}_i\theta_i v_i) = M_{iw}$$

$$\frac{\partial}{\partial z}(\bar{\rho}_w\theta_w v_w) = M_{wi} + M_{wv}$$

$$\frac{\partial}{\partial z}(\bar{\rho}_v\theta_v v_v) = M_{vw} \tag{25}$$

These point-scale equations are integrated over the snowpack depth D assuming that the ice matrix is at rest ($v_i = 0$). Replacing water fluxes across the boundaries by M and P (where P_t is precipitation rate), vapor fluxes by E_v and considering Eq. (6), the depthwise integration of the point-scale conservation equations through the snowpack yields the following depth averaged mass conservation equation for the snowpack at a point location over a snow-covered area:

$$D\frac{d}{dt}\bar{\rho}_s + \bar{\rho}_s\frac{dD}{dt} = \rho_w(P_t - E - M_r) \tag{26}$$

2.6. Summary of averaged conservation equations over the depth of a snowpack

The depth averaged energy equation through a snowpack at a point location over a snow-covered area was expressed by Eq. (9). This equation can be simplified further by first solving Eq. (11) for Z and then substituting the resulting expression for Z into Eq. (9). Then also combining Eq. (12) with Eq. (9) yields

$$\frac{d\bar{T}}{dt} = \frac{1}{\beta}(sw + G_1 - M) \tag{27}$$

where

$$\beta = [2A(C_p)_i\bar{T} - L_fW_0A + B(C_p)_i\bar{T}^2]\left(\frac{2k_1\bar{\rho}_s + 2k_2\bar{\rho}_s^3}{G_1^2}\right)$$

In summary, the depth averaged conservation equations through a snowpack at a point location over a snow-covered area may be expressed by Eq. (16) and Eq. (27) for energy and by Eq. (26) for mass. The next step is to extend these conservation equations over a snow-covered area.

3. Areal averaging of the conservation equations

The equations which were developed above to describe the energy and mass continuity represent the snowmelt dynamics at a point location in the snow cover area and characterize the depth averaged properties and processes within the snow pack at that location. One can consider these depth averaged equations as point location equations in relation to the snow cover area.

The averaging of differential equations over time or space has been traditionally performed by using the Leibnitz rule of differentiation. The approach that is applied here for averaging the point location conservation equations over the snow cover area is based on the perturbation of the 'snowmelt physics'. We can consider the point location equation as a perturbed mean equation. By the use of the Taylor expansion theory and ensemble averaging techniques we can obtain an approximate closed system of equations, depending on spatial statistical parameters of the snowmelt process. However, to apply the ensemble averaging technique to develop the areally averaged equations of the snowmelt physics, we make the fundamental assumption that the snowmelt process is spatially ergodic so that the ensemble averages may be equivalent to the areal averages.

The energy conservation equation can now be described by Eq. (16) and Eq. (27). In these equations, sw is given, $G_1 = A + BT_s$ where A and B are calculated from the meteorological data (Eq. (24), M is an unknown, and $\bar{T}$ and $\bar{\rho}_s$ are independent variables.

In an extended snow cover area, we can consider that $\bar{T}(t,\bar{x})$ and $\bar{\rho}(t,\bar{x})$ are also functions of the point location $\bar{x}$ in the snow cover. In the spatial averaging procedure, the equations will be expanded around the ensemble mean of these two variables, hypothesizing that the spatial variability of the snowmelt process is mainly given by the spatial variability of point location variables $\bar{T}(t,\bar{x})$ and $\bar{\rho}(t,\bar{x})$. These two variables are relevant in the physics of the melting processes. In a broad sense, it can be said that snow temperature dictates the direction and magnitude of most energy fluxes across the boundaries, and snow density is the bulk parameter that best describes the internal properties and physical state of the snowpack.

3.1. Equations for the areal means

To simplify the averaging procedure Eq. (27) and Eq. (16) can be written respectively in the forms

$$\frac{d\bar{T}}{dt} = a_{(T,\rho)} \text{ and } \frac{d\bar{\rho}}{dt} = b_{(T,\rho)}$$

where the subscript s in $\bar{\rho}_s$ is dropped for mathematical convenience in the following. Under ergodicity assumption, the depth averaged snow temperature $\bar{T}$ can be written in terms of Taylor series expansion around the areal average snow temperature $\langle\bar{T}\rangle$ and areal average snow density $\langle\bar{\rho}\rangle$ as

$$\frac{d\bar{T}}{dt} = [a_{(T,\rho)}]_{(0)} + \left\{\frac{\partial[a_{(T,\rho)}]}{\partial T}\right\}_{(0)}(\bar{T}-\langle\bar{T}\rangle) + \left\{\frac{\partial[a_{(T,\rho)}]}{\partial \rho}\right\}_{(0)}(\bar{\rho}-\langle\bar{\rho}\rangle) + \frac{1}{2}\left\{\frac{\partial^2[a_{(T,\rho)}]}{\partial T^2}\right\}_{(0)}(\bar{T}-\langle\bar{T}\rangle)^2 + \frac{1}{2}\left\{\frac{\partial^2[a_{(T,\rho)}]}{\partial \rho^2}\right\}_{(0)}(\bar{\rho}-\langle\bar{\rho}\rangle)^2 + \left\{\frac{\partial^2[a_{(T,\rho)}]}{\partial T\partial \rho}\right\}_{(0)}(\bar{T}-\langle\bar{T}\rangle)(\bar{\rho}-\langle\bar{\rho}\rangle) + O\left[(\bar{T}-\langle\bar{T}\rangle)^3,(\bar{\rho}-\langle\bar{\rho}\rangle)^3\right] \tag{28}$$

where the subscript (0) denotes that the function within the brackets is evaluated at the mean values ($\bar{T}=\langle\bar{T}\rangle, \bar{\rho}=\langle\bar{\rho}\rangle$), and $O[]$ indicates the truncation error, which is of the order of the first omitted term.

Considering that the terms within brackets take deterministic values when evaluated at (0), and $\langle(\bar{T}-\langle\bar{T}\rangle)\rangle = 0$ and $\langle(\bar{\rho}-\langle\bar{\rho}\rangle)\rangle = 0$, the ensemble average of the Eq. (28) can be written as

$$\frac{d\langle\bar{T}\rangle}{dt} = [a_{(T,\rho)}]_{(0)} + \frac{1}{2}\left\{\frac{\partial^2[a_{(T,\rho)}]}{\partial T^2}\right\}_{(0)}\mathrm{Var}(\bar{T}) + \frac{1}{2}\left\{\frac{\partial^2[a_{(T,\rho)}]}{\partial \rho^2}\right\}_{(0)}\mathrm{Var}(\bar{\rho}) + \left\{\frac{\partial^2[a_{(T,\rho)}]}{\partial T\partial \rho}\right\}_{(0)}\mathrm{Cov}(\bar{T},\bar{\rho}) \tag{29}$$

Under the ergodicity assumption, Eq. (29) describes the behavior of the areally averaged snow temperature. The error involved in the approximation is of the order of the third moment of $\bar{T}$ and $\bar{\rho}$. Following the same procedure for the depth averaged equation of the rate of change in snow density an equation describing the behavior of the areally averaged snow density can be obtained as

$$\frac{d\langle\bar{\rho}\rangle}{dt} = [a_{(T,\rho)}]_{(0)} + \frac{1}{2}\left\{\frac{\partial^2[b_{(T,\rho)}]}{\partial T^2}\right\}_{(0)}\mathrm{Var}(\bar{T}) + \frac{1}{2}\left\{\frac{\partial^2[b_{(T,\rho)}]}{\partial \rho^2}\right\}_{(0)}\mathrm{Var}(\bar{\rho}) + \left\{\frac{\partial^2[b_{(T,\rho)}]}{\partial T\partial \rho}\right\}_{(0)}\mathrm{Cov}(\bar{T},\bar{\rho}) \tag{30}$$

It may be noticed that Eq. (29) and Eq. (30) depend on the variables $\langle\bar{T}\rangle$, $\langle\bar{\rho}\rangle$, $\mathrm{Var}(\bar{T})$, $\mathrm{Var}(\bar{\rho})$ and $\mathrm{Cov}(\bar{T},\bar{\rho})$. Here, $\langle\bar{T}\rangle$ is the areal mean snow temperature, $\mathrm{Var}(\bar{T})$ is the areal variance of the snow temperature, $\langle\bar{\rho}\rangle$ and $\mathrm{Var}(\bar{\rho})$ are respectively the areal mean and areal variance of the snow density, and $\mathrm{Cov}(\bar{T},\bar{\rho})$ is the areal covariance between snow temperature and snow density, under the ergodicity assumption. To close the system of Eq. (29) and Eq. (30) it is necessary to develop equations for the variance and covariance terms.

3.2. Equations for the areal variances

Applying the definition of the variance,

$$\frac{\mathrm{dVar}(\bar{T})}{\mathrm{d}t}=\frac{\mathrm{d}}{\mathrm{d}t}(\langle\bar{T}^2\rangle-\langle\bar{T}\rangle^2) \tag{31}$$

Expanding the right-hand side of Eq. (31) as a Taylor series around $\langle\bar{T}\rangle$ and $\langle\bar{\rho}_s\rangle$, neglecting third- and higher- order terms, and denoting $a(T,\rho)=(\mathrm{d}\bar{T})/(\mathrm{d}t)$ results in

$$\frac{\mathrm{dVar}(\bar{T})}{\mathrm{d}t}=2\mathrm{Var}(\bar{T})\left\{\frac{\partial[a_{(T,\rho)}]}{\partial T}\right\}_{(0)}+2\mathrm{Cov}(\bar{T},\bar{\rho})\left\{\frac{\partial[a_{(T,\rho)}]}{\partial\rho}\right\}_{(0)} \tag{32}$$

Eq. (32) is an equation for the areal variance of snow temperature as a function of the first derivative of the point location snow temperature which is evaluated at the areal mean value. A similar procedure can be applied to the areal variance of the snow density to produce the following explicit equation for the areal variance of snow density under the assumption of ergodicity of the snow-covered region:

$$\frac{\mathrm{dVar}(\bar{\rho})}{\mathrm{d}t}=2\mathrm{Var}(\bar{\rho})\left\{\frac{\partial[b_{(T,\rho)}]}{\partial\rho}\right\}_{(0)}+2\mathrm{Cov}(\bar{T},\bar{\rho})\left\{\frac{\partial[b_{(T,\rho)}]}{\partial T}\right\}_{(0)} \tag{33}$$

where $b_{(T,\rho)})=\frac{\mathrm{d}\bar{\rho}}{\mathrm{d}t}$.

3.3. Equation for the areal covariance

By definition, the time derivative of the areal covariance can be written as

$$\frac{\mathrm{dCov}(\bar{T},\bar{\rho})}{\mathrm{d}t}=\frac{d}{\mathrm{d}t}\langle(\bar{\rho}-\langle\bar{\rho}\rangle)(\bar{T}-\langle\bar{T}\rangle)\rangle \tag{34}$$

Expanding the right-hand side of Eq. (34) around the areal mean values in terms of Taylor series and applying the same considerations used for the mean and variance, results in the following equation for the areal covariance:

$$\begin{aligned}\frac{\mathrm{dCov}(\bar{T},\bar{\rho})}{\mathrm{d}t}=&\mathrm{Var}(\bar{T})\left\{\frac{\partial[b_{(T,\rho)}]}{\partial T}\right\}_{(0)}+\mathrm{Var}(\bar{\rho})\left\{\frac{\partial[b_{(T,\rho)}]}{\partial\rho}\right\}_{(0)}\\&+\mathrm{Cov}(\bar{T},\bar{\rho})\left\{\frac{\partial[a_{(T,\rho)}]}{\partial T}+\frac{\partial[b_{(T,\rho)}]}{\partial\rho}\right\}_{(0)}\end{aligned} \tag{35}$$

The set of ordinary differential equations, Eqs. (29), (30), (32), (33) and (35), constitutes a closed system which depends on areally averaged variables. This system of equations originates from the depth-averaged dynamics of snowmelt, expressed as a point location process.

3.4. Freezing depth

The freezing depth Z can be averaged over the snow cover area using the same Taylor expansion method. Combining Eq. (11) and Eq. (12), the expression for Z can

be written as

$$Z=\frac{2(k_1+k_2\bar{\rho}_s^2)\bar{T}}{G_1}=c_{(T,\rho)} \tag{36}$$

Expanding Z around the areal means yields the relationship

$$\langle Z\rangle=[c_{(T,\rho)}]_{(0)}+\frac{1}{2}\mathrm{Var}(\bar{T})\left\{\frac{\partial^2[c_{(T,\rho)}]}{\partial T^2}\right\}_{(0)}+\frac{1}{2}\mathrm{Var}(\bar{\rho})\left\{\frac{\partial^2[c_{(T,\rho)}]}{\partial \rho^2}\right\}_{(0)}+\mathrm{Cov}(\bar{T},\bar{\rho})\left\{\frac{\partial^2[c_{(T,\rho)}]}{\partial T\partial \rho}\right\}_{(0)} \tag{37}$$

3.5. Solution to the mass equation

If there is no snowmelt, i.e. whenever $\langle\bar{T}\rangle < 0°C$, Eqs. (29), (30), (32), (33) and (35) can be solved for $\langle\bar{T}\rangle$, $\langle\bar{\rho}\rangle$, $\mathrm{Var}(\bar{T})$, $\mathrm{Var}(\bar{\rho})$ and $\mathrm{Cov}(\bar{T},\bar{\rho})$.

Once $\langle\bar{\rho}\rangle$ is known at the beginning and end of a computational time interval, the depth averaged mass conservation equation, Eq. (26), then becomes linear with respect to the spatially averaged depth of the snowpack, $\langle D\rangle$ when its ensemble average (areal average under ergodicity) is taken. That is, the ensemble averaging of Eq. (26) under known $\langle\bar{\rho}\rangle$ yields

$$\langle D\rangle\frac{\mathrm{d}}{\mathrm{d}t}\langle\bar{\rho}_s\rangle+\langle\bar{\rho}_s\rangle\frac{\mathrm{d}\langle D\rangle}{\mathrm{d}t}=\rho_w(\langle P_t\rangle-\langle E\rangle-\langle M_r\rangle) \tag{38}$$

which is the areally averaged mass conservation equation over a snow cover area. Expressing Eq. (38) in finite differences, it can be solved for $\langle D\rangle$ at the end of the interval. If the solution of the equation system Eqs. (29), (30), (32), (33) and (35) results in $\langle\bar{T}\rangle \geq 0°C$, then the snowmelt $\langle M\rangle$ is calculated from this equation system under $\langle\bar{T}\rangle = 0$.

4. Model formulation

The final formulation of the spatial approach is obtained by taking derivatives of $a_{(T,\rho)}$, $b_{(T,\rho)}$ and $c_{(T,\rho)}$ with respect to $\bar{T}$ and $\bar{\rho}$ and substituting these derivatives into Eqs. (29), (30), (32), (33), (35) and (37). These operations lead to very involved algebraic expressions which will be omitted for brevity.

It can be noticed that the point location equations are a particular case of the areally averaged equations system. In a point location situation the variances and covariances are zero and the mean spatial parameters take the point values. Consequently, the areally averaged system of equations is reduced to the system given by the depth averaged equations representing a point location process. On the other hand, when the application is extended over an area, the areal variables $\langle\bar{T}\rangle$, $\langle\bar{\rho}\rangle$, $\mathrm{Var}(\bar{T})$, $\mathrm{Var}(\bar{\rho})$ and $\mathrm{Cov}(\bar{T},\bar{\rho})$ will adjust to the scale of the process by taking values dictated by the fluctuations in time and

space of the input meteorological variables and by how these areal variables are related to the physics of the melt process.

The initial conditions are specified for $\langle \bar{T} \rangle$, $\langle \bar{\rho} \rangle$, $\langle D \rangle$, $\mathrm{Var}(\bar{T})$, $\mathrm{Var}(\bar{\rho})$ and $\mathrm{Cov}(\bar{T}, \bar{\rho})$. The energy balance is calculated using areally averaged meteorological data. This information may come from point location observations or from any other means such as satellite information or mesoscale climatic models.

The system of equations is solved using a Runge–Kutta numerical method for each time interval. Using Eq. (37), the areal average snow freezing depth $\langle Z \rangle$ is calculated. If $\langle Z \rangle$ is out of the interval $(0 < \langle Z \rangle < \langle D \rangle)$ then $\langle Z \rangle$ is forced to take the extreme admissible value of the interval, and $\langle \bar{T} \rangle$ is recalculated by Newton method applied to Eq. (37). This new value of $\langle \bar{T} \rangle$ is then used to solve the equation system for the final values of the areal variables during the time interval. Finally, Eq. (38) is solved for $\langle D \rangle$ at the end of the time interval.

5. Model testing

The main difficulty in testing an areal-scale model is acquiring spatially distributed data records. Meteorological data for air temperature, relative humidity, radiation and wind velocity are required at several sites of the area. The areal average of these values are the inputs of the areal-scale model. Additionally, distributed observations of snowmelt, snow temperature and snow density should be available to compare with the results obtained by the areal-scale model ($\langle \bar{T} \rangle$, $\mathrm{Var}(\bar{T})$, $\langle \bar{\rho} \rangle$, $\mathrm{Var}(\bar{\rho})$, $\langle M \rangle$). However, some of these variables are not routinely observed. As a consequence, the model developed in this study had to be tested by the regular information available for a typical snow-covered catchment.

The area selected for model testing was Scott Valley Basin in Northern California. Most of the information and data required from Scott Valley Basin were compiled in a previous study by Van der Heydt (1991), who applied a point location snowmelt model (which will be called Model L) to this area. The fact that the model developed in this study had to be tested by data from few observation point locations forced us to prepare three different tests.

5.1. Study area characteristics

The Scott Valley watershed is a 1600^2 km basin located in Northern California (Siskiyou County). The topography of the region is rugged, having elevations from 2500 m at the peaks to 500 m at the basin outlets. Snow accumulation occurs as a result of storms coming from the Pacific during winter. Snowmelt takes place during interstorm periods and in spring.

There are two snow pillow sites within the basin at the southern end of the watershed, namely Middle Boulder 3 and Scott Mountain. A further three observation point sites outside the basin, at Peterson Flat, Mumbo and Big Flat, are close enough to provide valid information for the study area. At these five stations cumulative precipitation is also recorded. Data are registered by sensors that transmit the signal at periodic intervals via the Geostationary Operational Environmental Satellite to a central computer facility in Sacramento, California.

Diurnal fluctuations of snow water equivalent (SWE) readings as a result of temperature-induced effects make a determination of the 3 h incremental melt impossible. It is convenient therefore to use daily incremental SWE as a representative measure of the snow depth variations.

Three remote automated weather stations (RAWS) in Scott Valley Basin measure hourly relative humidity, precipitation, air temperature, wind speed and direction. These three stations are located at Collin's Baldy (1670 m), Quartz Hill (1200 m) and Callahan (500 m). Additionally, at Scott Mountain air temperature is measured and recorded every 3 h.

Total global solar radiation is monitored at Red Bluff by Pacific Gas and Electric Company. A spectral pyranometer measures total horizontal solar radiation yielding 30 min average values. Fractional sky cover and cloud base elevation are recorded at Redding, Siskiyou and Montague airports.

The shortwave radiation data (*sw*) which were used in model testing studies, was prepared by Van der Heydt (1991), who calibrated a radiation model using Red Bluff solar radiation. The calibrated atmospheric transmissivity parameter was found to be 0.68. This is in agreement with Williams (1972). Subsequent adjustment to the basin was made possible by using Redding and Montague airport information on cloudiness. The albedo was computed by using an exponential decay function of albedo with time since the last snowfall (Kondo and Yamazaki, 1990).

5.2. Case 1: point location simulation

The first test was directed toward validating the formulated method applied as a point location model. By setting the variances and covariances to zero and considering $\langle \bar{T} \rangle$ and $\langle \bar{\rho} \rangle$ as point location variables, the result of the system will correspond to a point location solution.

The simulation period chosen is 6–19 April 1986, when no snow accumulation occurred. The model was applied to the Scott Mountain site. For this particular location, most of the snowmelt occurred during 6–19 April. By 19 April snow depth had decreased from 39 cm to about 2 cm. The zero time for the simulation corresponds to 6 April at 04:00. For model computations a 15 min interval was used according to the data availability. No interpolation of the observed data (air temperature, relative humidity, wind and shortwave incoming radiation) was required.

The values given to the parameters of the model were related to the conditions existing in Scott Mountain during the period 6–19 April. The emissivity of the snow surface was taken $\epsilon_s = 0.99$, the water content of snow at 0°C was taken as $W_0 = 0.10$ (this value was suggested by Kondo and Yamazaki (1990)), the bulk coefficients for turbulent transfer were taken as $D_h = 0.0030$ and $D_e = 0.0015$ (Male and Gray, 1981), the effective thermal conductivity coefficients were taken as $k_1 = 0.25$ and $k_2 = 25$ in Eq. (12) (units cal cm^{-1} h^{-1} K^{-1}), the viscosity coefficient was taken as $\eta_0 = 20$ cm h^{-1}, and $k_0 = 21$ cm^3 g^{-1} in Eq. (16) (Anderson, 1976). The initial values of the state variables were fixed at $\bar{T} = -1$°C, $\mathrm{Var}(\bar{T}) = 0$, $\bar{\rho}_s = 0.38$ g cm^{-3}, $\mathrm{Var}(\bar{\rho}) = 0$, $\mathrm{Cov}(\bar{\rho}, \bar{T}) = 0$, $D = 39$ cm.

In Fig. 3, the values of snow surface temperature during the first 5 days of the simulation period calculated by the model developed in this study are compared with the results

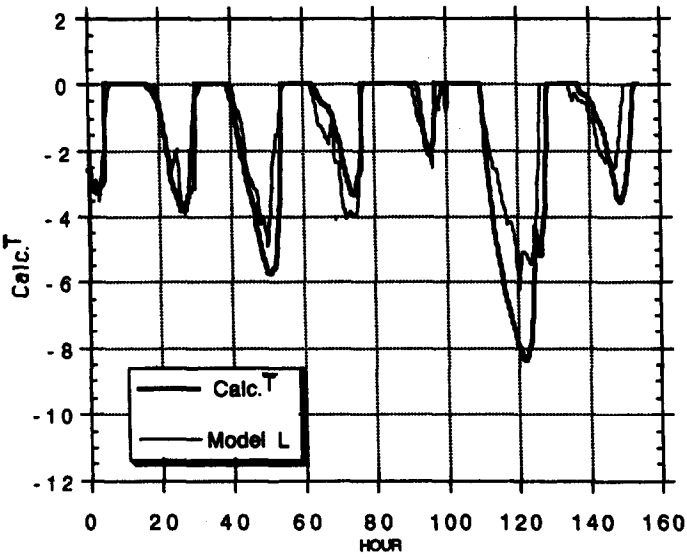

Fig. 3. Surface snow temperature comparison.

predicted by Model L (Van der Heydt, 1991). A periodic curve was obtained as a result of the incoming energy fluctuations during the day–night diurnal cycle. Although there are some differences in the curve shapes and magnitudes of temperature at certain points in time, there is a significant agreement between the two models.

Fig. 4 shows the comparison of daily cumulative snowmelt values. According to Fig. 4,

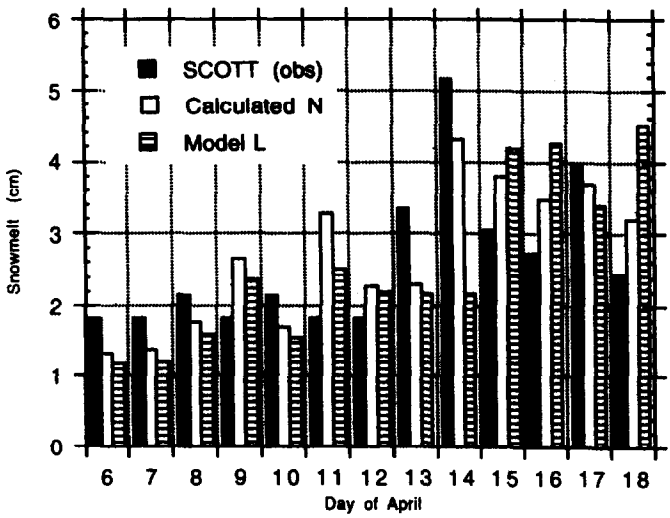

Fig. 4. Comparison of snowmelt estimated by the developed model in its point location form (Calculated N), observed, and snowmelt estimated by Model L.

the simulation of the observed values at Scott Mountain site by the developed point location model of this study (denoted by 'calculated N') is satisfactory. The discrepancies between the snowmelt calculated by the developed model and the Van der Heydt model (Model L) predictions can be explained by several factors. In Model L, equations are solved analytically, whereas in the point location model of this study a numerical solution is obtained. This may be the reason for the slightly longer melting periods obtained by our point location model in Fig. 3 (as compared with Model L), which will contribute to higher snowmelt cumulative yields. During the melting periods shortwave radiation and turbulent transfer of heat to the atmosphere dominate the energy balance. In the turbulent transfer process the values of the parameters involved may be different in the two models, increasing the snowmelt calculated by our point location model.

The general agreement between the two models and observed data confirms that the original point location physics representation of the melting process by our model is reasonably correct and the assumptions and simplifications made in the procedure are acceptable. In summary, it can be said that, based on the results obtained from the data available, the developed point location snowmelt model performed satisfactorily.

5.3. Case 2: tests based upon areal model simulations

To test the areal snowmelt model it is important to compare the calculated areal mean

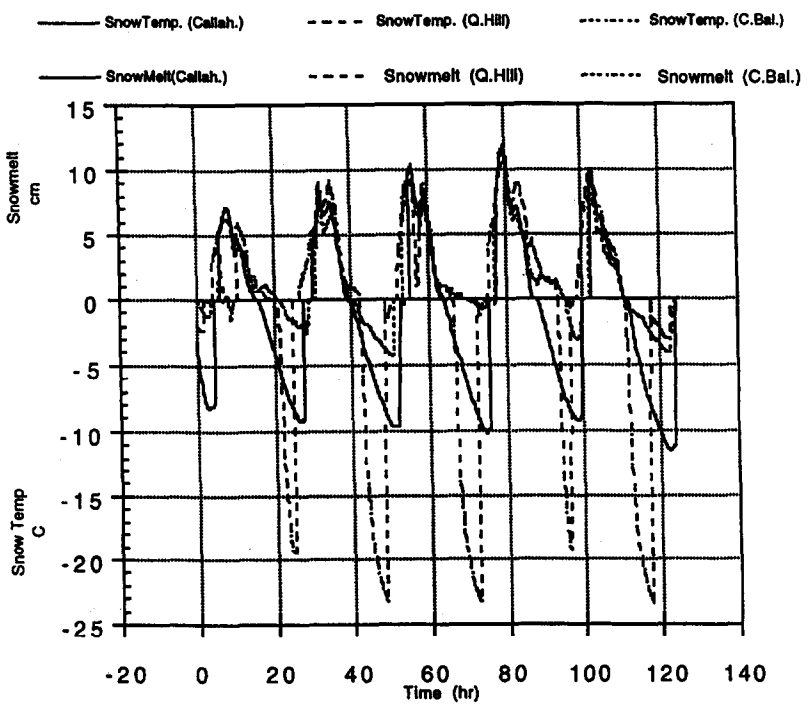

Fig. 5. Snowmelt (positive) and snow temperature (negative) calculated by the point location form of the model at three locations in Scott Valley Basin.

snow temperature, snow temperature areal variance and areal mean snowmelt with the corresponding observed quantities. However, only the snowmelt is actually observed in the Scott Valley Basin. Consequently, a simulation of point location snow temperature was performed at three locations in Scott Basin by utilizing the point location model developed in this study. Meteorological data for air temperature, relative humidity, wind speed and solar radiation were available for three sites, at Callahan, Collin's Baldy and Quartz Hill. The simulated snow temperature and snowmelt at these three locations were used to calculate the areal arithmetic average of $\bar{T}$ and M, and the variance of $\bar{T}$. Although these values were simulated by the point location model we will denote these averages hypothetically as 'observed' average $\bar{T}$ and M and 'observed' variance of snow temperature.

The areally averaged values of air temperature, relative humidity, wind velocity and shortwave radiation observed at these three locations were then used as input data to the areal snowmelt model to estimate $\langle\bar{T}\rangle$, $\langle M\rangle$ and $\mathrm{Var}(\bar{T})$. Finally, the calculated areal variables and those 'observed' ones obtained from averaging point location model simulations were compared.

Fig. 5 represents the point location model calculated snowmelt and snow temperatures at Callahan, Collin's Baldy and Quartz Hill. The parameter values used for the calculations are similar to those used in Case 1.

In Fig. 6, the areal mean value of snow temperature, $\langle\bar{T}\rangle$, obtained through the areal model is compared with the 'observed' temperature, which was obtained from averaging

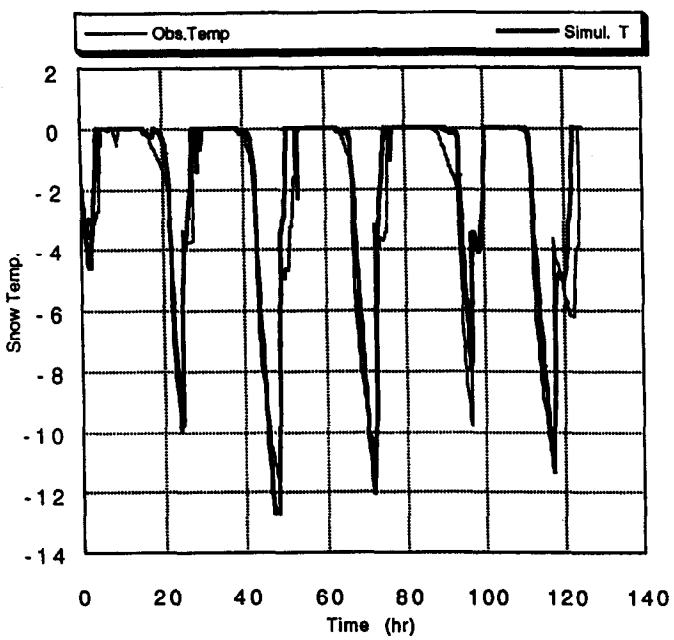

Fig. 6. Simulated areal mean temperature, obtained from areal snowmelt model, vs. the 'observed' temperature, obtained from averaging the temperatures simulated using the point location model at three sites in Scott Valley Basin.

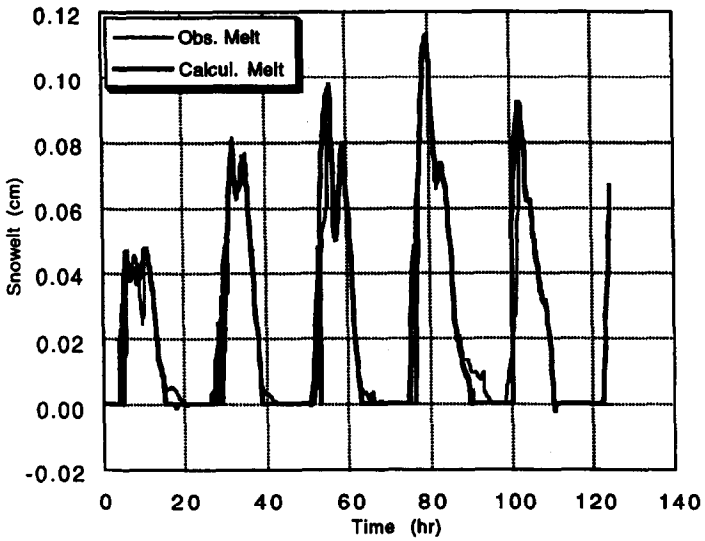

Fig. 7. Comparison of snowmelt calculated using the areal model (Calcul. Melt) with that calculated from averaging the snowmelt simulated using the point location model at three sites in Scott Valley Basin (Obs. Melt).

the point location model simulated temperatures at above-mentioned three locations. Correspondingly, in Fig. 7 calculated snowmelt is compared with the 'observed' snowmelt which was obtained from averaging the point location model simulated snowmelt at the three locations. In both cases there is good agreement. There is no 'calibration parameter' in the areal model. The initial values can be adjusted within a certain interval. In this case,

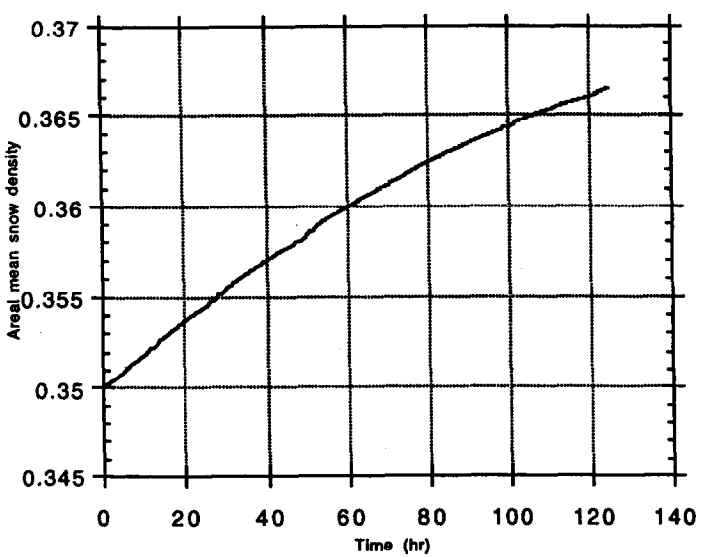

Fig. 8. Areal mean snow density calculated using the areal model.

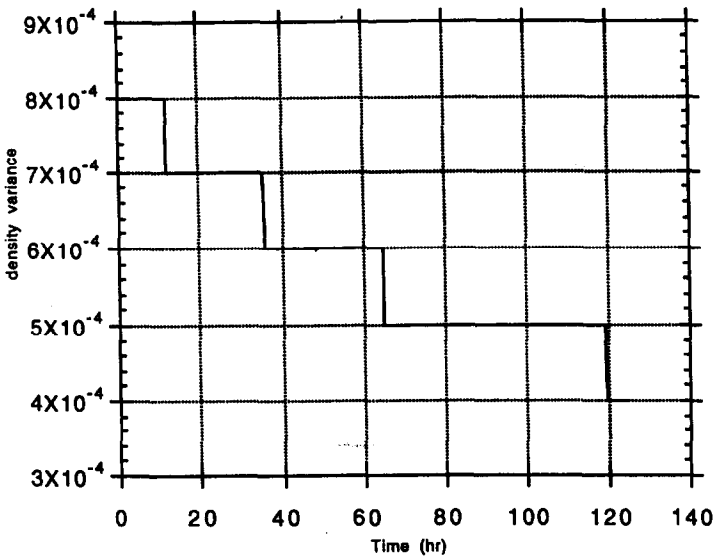

Fig. 9. Snow density areal variance calculated using the areal model.

the initial conditions were $\langle\bar{T}\rangle=-2.0$, $\mathrm{Var}(\bar{T})=4.0$, $\langle\bar{\rho}\rangle=0.35$, $\mathrm{Var}(\bar{\rho})=0.001$, $\mathrm{Cov}(\bar{T},\bar{\rho})=0.0$.

Analyzing the performance of the developed model, it was noticed that the effects of the initial values of $\langle\bar{T}\rangle$, $\mathrm{Var}(\bar{T})$, $\langle\bar{\rho}\rangle$, $\mathrm{Var}(\bar{\rho})$, and $\mathrm{Cov}(\bar{T},\bar{\rho})$ were very different. Whereas the initial value of $\langle\bar{T}\rangle$ influenced the first daily cycle, the initial value of $\langle\bar{\rho}\rangle$ affected the whole calculation period. From Fig. 8, it can be seen that $\langle\bar{\rho}\rangle$ does not have the cyclic pattern shown by $\langle\bar{T}\rangle$ in Fig. 6. On the contrary, the smooth change of $\langle\bar{\rho}\rangle$ is mostly due to compacting through time. This affects the dynamics throughout the simulation period, in accordance with the nature of snowmelting process. In Fig. 8, the tiny deviations of $\langle\bar{\rho}\rangle$ from the main exponential tendency of the curve is due to variation in $\langle\bar{T}\rangle$ and can be barely noticed. The exponential dependence of $\langle\bar{\rho}\rangle$ on $\langle\bar{T}\rangle$, expressed in Eq. (16), is manifested when the same temperature persists for an extended period of time. The value of $\langle\bar{\rho}\rangle$ is also sensitive to $\mathrm{Var}(\bar{\rho})$, which affects the rate at which $\langle\bar{\rho}\rangle$ changes. The tendency of $\mathrm{Var}(\bar{\rho})$ is to decrease with time (see Fig. 9), indicating that the compacting effect tends to cause a more uniform snow cover density. The range of plausible values for $\mathrm{Var}(\bar{\rho})$ is of the order of 0.001 g cm^{-3} h^{-1}.

The temperature areal variance curves displayed in Fig. 10 show some differences in the magnitude of the peaks. $\mathrm{Var}(\bar{T})$ is very sensitive to the initial conditions, and perhaps there exist different combinations of initial values that may yield a better fit. Another consideration is the number of point locations from which the 'observed' variance is estimated. Three sites is a low sample number. Also, they may not be completely representative of the watershed or the area covered by the input data. However, the shape of both curves, their trend and location of the peaks are in agreement.

The areal covariance of snow density with snow temperature has a fluctuating pattern (see Fig. 11). Although the values taken by the covariance are low in magnitude, they

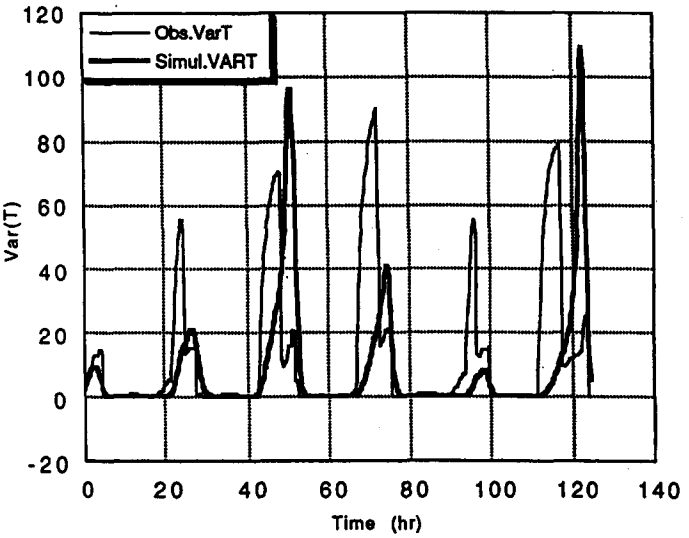

Fig. 10. Comparison of snow temperature areal variance calculated using the areal model (Simul. VART) with that calculated from the snow temperatures simulated using the point location model at three sites in Scott Valley Basin (Obs. VarT).

affect the dynamics. The covariance may be ignored in the perturbation procedure, approximating the snowmelt physics equations by only considering the variance terms. However, in that case (setting $\mathrm{Cov}(\bar{\rho}, \bar{T}) = 0$ and ignoring the equation for the covariance) it was seen that stability problems occur, causing $\mathrm{Var}(\bar{T})$ to take negative values, which in turn leads to divergence problems.

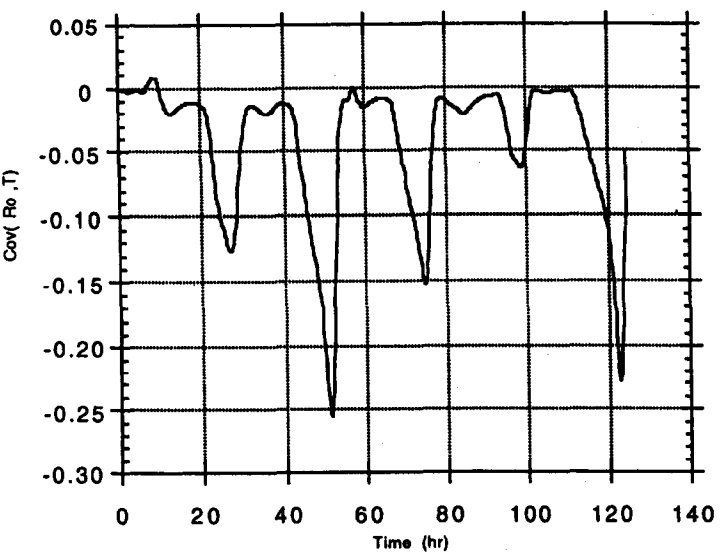

Fig. 11. Areal covariance of snow density with snow temperature calculated using the areal model.

The discrepancies observed between the curves in Fig. 7 occur mainly at the beginning and end of a melting cycle. The reason for this may be related to the assumption that melts occur only when $\langle T \rangle = 0$. This is true at a point location scale but may not be true at areal scale. Some snowmelt can be expected even when $\langle T \rangle$ is below freezing, especially when the mean temperature is close to the freezing temperature.

5.4. Case 3: areal model predictions vs. observations

A more realistic application was carried out to test the areal model's performance. All the information available for the Scott Valley Basin area were used to compare observed areally averaged snowmelt with the areal mean snowmelt calculated by using the method developed in this study. The developed areal model used as its input the averaged meteorological data for the basin, and the results were compared with areally averaged observed snowmelt for the area.

The calculation period used was again from 6 April at 04:00 h to 18 April at 12:00 h, and the computational time interval was fixed to be 15 min. The variability of the observed snowmelt in time and space over the Scott Valley Basin study area is shown in Fig. 12. Four out of five stations present similar values whereas the Middle Boulder station significantly exceeds the others in magnitude. Given that no information exists on how representative these observation sites are of the Scott Valley Basin area, Middle Boulder was included in the averaging with the same weight as the other stations.

Several runs were performed to find the best combination of initial values to fit the daily cumulative observed and five-station areally averaged snowmelt. In the calibration process, emphasis was put on the initial conditions rather than on the parameter values such as bulk turbulent transfer coefficients D_e and D_h, albedo coefficient, and snow water

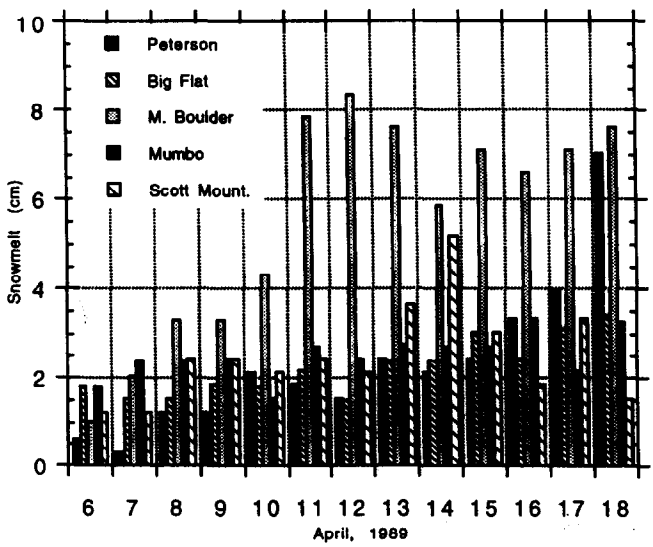

Fig. 12. Observed snowmelt at five stations in the Scott Valley Basin study area.

content W_0. Much can be said about the parameterization of the snowpack properties and the energy fluxes. The parameter values can always be improved, depending on the accuracy and spatial density of the input data and the observed output variables. However, we will concentrate on the results related to the spatial features of the model, the central topic of this research. Consequently, the parameter values were taken from the literature.

During the calibration runs, it was observed that increasing the initial value of $\langle\bar{\rho}\rangle$ produces lower peaks in $\langle\bar{T}\rangle$ and Var($\bar{T}$). An increase of density is associated with a quadratic increase in thermal conductivity. In a more conductive medium, a deeper snow layer becomes active, keeping the fluctuations in temperature within a smaller range. As a consequence, a decrease in Var($\bar{T}$) may be expected when snow density increases.

It was also observed that Var($\bar{T}$) is very sensitive to the initial values of Var($\bar{\rho}$). Increasing Var($\bar{\rho}$) by 0.001 results in high peaks of Var($\bar{T}$). Again, this effect seems to be controlled by the relation between $\bar{\rho}$ and λ_e, which turns out to be very important in the spatial dynamics. By adjusting the initial values it was possible to reproduce fairly well the areally averaged observed snowmelt.

In Fig. 13, the areal model predicted and observed areally averaged daily cumulative snowmelt are displayed. According to this figure there is good agreement between predicted and observed daily melts. However, the areal model predictions, in general, underestimate the observed areally averaged snowmelt. The observed snowmelt during the study period accumulates to 49 cm whereas the predicted value is 46 cm. This difference

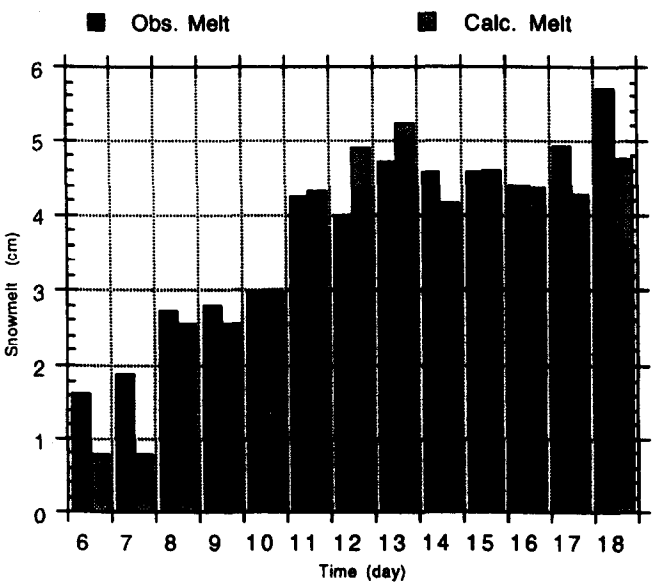

Fig. 13. Comparison of measured areally averaged (five station averaged) snowmelt (Obs. Melt) with the areally averaged snowmelt predicted using the areal model (Calc. Melt).

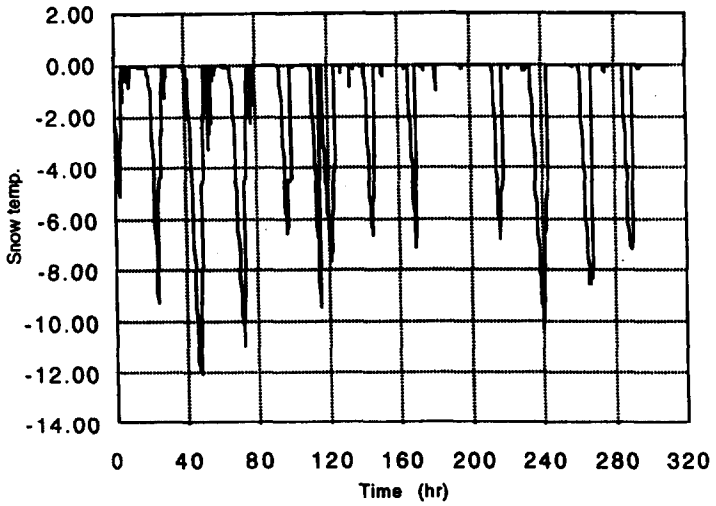

Fig. 14. Model calculated areal average snow temperature at Scott Valley Basin.

may be caused by several factors such as incorrect parameter values, measurement errors and the assumption stipulating that snowmelt occurs only when $\langle T \rangle = 0°C$.

At the ninth simulation day (approximately 190 h) the snow temperature (Fig. 14) is maintained at 0°C during the night. This is a particularly long period during which the snow stayed at the same temperature, altering the compacting rate, and producing a visible effect in the snow density curve (Fig. 15).

According to Fig. 13, the areal model seems to be capable of simulating the areal average snowmelt for the conditions presented in Scott Basin. Eventually, a better fit

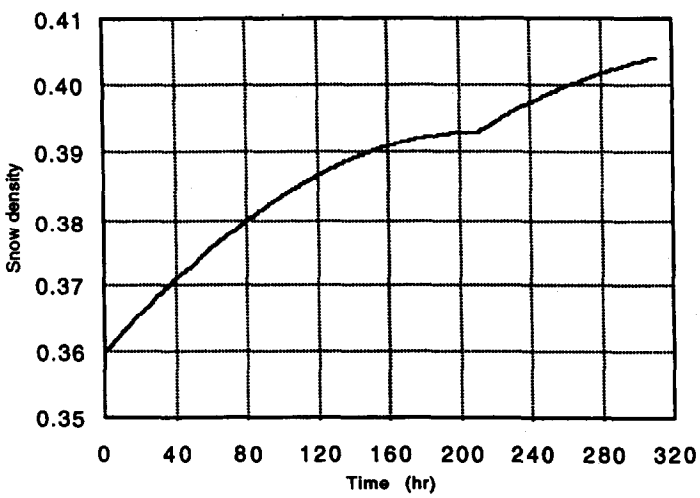

Fig. 15. Model calculated areal average snow density at Scott Valley Basin.

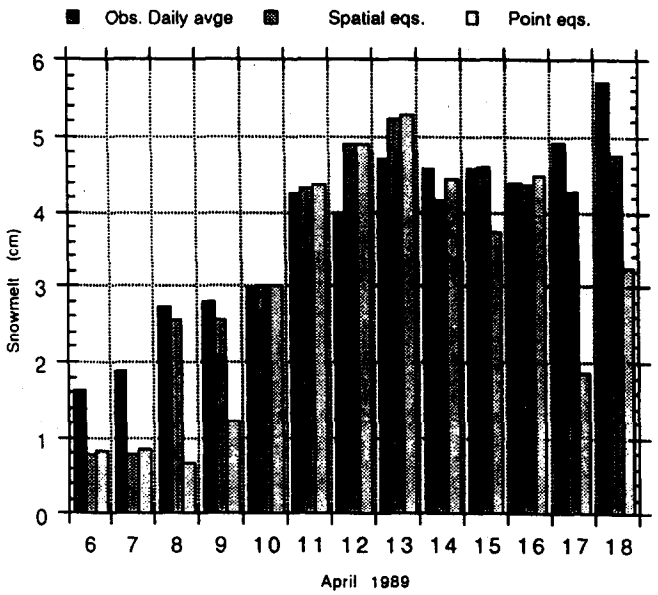

Fig. 16. Comparisons of observed areally averaged snowmelt (Obs. Daily avg.) and areal mean snowmelt predicted by areal model (Spatial eqs.) and point location model (Point eqs.).

could be obtained by developing a parameter estimation scheme based upon topographical data, satellite information, wind profiles, stability parameters, vegetation, etc. However, the information which was available and which was utilized in the application of the areal model is the usual data a hydrologist would have for any real-life situation.

Finally, a comparison of areally averaged snowmelt resulting from the observations, from the areal model and from the point location modeling approach was made. For this, the same input data as used to calculate $\langle M \rangle$ were also applied to estimate M at a point location by considering the areal variance and covariance terms as zero. The point location modeling represents the traditional approach in which the snowmelt is estimated by using the point location physical relationships under spatially distributed inputs. Point location model predictions of snowmelt were first obtained at the five above-mentioned sites in Scott Valley Basin. Then these site-specific predictions were averaged over the five sites to obtain areally averaged predictions of snowmelt in Scott Valley Basin by the point location modeling approach.

In Fig. 16 the observed, the areal model calculated and point location model calculated areal mean daily snowmelt values can be compared. The accumulated value for M calculated by the point location modeling approach during the simulation period sums to 39 cm, which is below the other two cumulative values (46 for areal model and 49 for observations). From this comparison it may be deduced that the cumulative daily snowmelt predictions from the areal model are equal to or better than the corresponding predictions from the point location modeling approach.

6. Concluding remarks

The following conclusions and recommendations for future investigations may be stated:

1. The results of the areal model developed in this study are in agreement with the observed data. The magnitude and trend of the measured daily snowmelt (basin averages) are reproduced satisfactorily by our areal model. Also, the developed model performs well as a point location model when its results are compared with observed point location snow water equivalent (SWE) data and with the results from another point location model. Therefore, the model performs well, independently of the spatial scale of application, i.e. either at point location scale or at areal scale.
2. There is evidence that the areal model captures the spatial variability of the snow cover. The areal snow temperature variance from the developed model agrees with the areal temperature variance estimated by point location simulations. The areal model includes the spatial variability of snow temperature and snow density in the snow cover. This is an important departure from the traditional point location application. Consequently, the results obtained by the areal model differ from those obtained by the traditional point location model. Better concordance with areal observations is obtained by the areal model.
3. Although the results of the areal model are in agreement with the observed data, the model still needs to be tested over a wide range of snow cover and climate conditions. In addition, reliable hourly SWE data are necessary for comparison with model results at time scales appropriate for the snowmelt dynamics. A large number of observation points that provide meteorological and snow cover data are essential for a conclusive validation of the developed approach. An intermediate spatial scale of application between point location and basin areal scale is necessary to evaluate how the areal model depends on the spatial scale of the simulation.
4. The averaging procedure applied in this study to the snowmelt processes allows for the modifications to the method utilized in estimating the energy balance. There is a wide range of available energy budget techniques, depending on which components of the budget are measured directly and which empirical equations are used to estimate the other components. Depending upon the purpose of the application and on the available data, other techniques may be more adequate than the energy budget method which was used in this research. For example, a temperature index approach may be used when only air temperature measurements are available.
5. The movement of water within the snowpack is neglected in this study. The assumption of instantaneous release of water out of the pack is not very realistic. To make it more realistic, an expression for the flow moving through the snow needs to be added in the future to the snowmelt models which were developed in this study. The flow of water through the snow is subject to properties that depend on the metamorphic state of the snow. This makes it difficult to estimate the flow. At present, the developed models circumvent this problem by calculating a mean freezing depth which separates dry and wet snow layers. The freezing depth defines a boundary condition for the water that flows in the wet layer.

6. Future research is necessary to determine when, where, and how the snow cover area should be subdivided, so as to make better use of the areal snowmelt model. Although the equations are expressed as functions of the spatial variability of the main physical properties of the snow cover, some differences in the characteristics of the snow cover area may justify subdivision of the study area. Seasonal and perennial snow covers are subject to different rates of compaction and different density–heat conductivity relationships. Climatic differences on the windward and leeward sides of a mountainous system should also be considered. Even shortwave radiation captured by the snow may be very dissimilar from one snow cover area to another, owing to differences in albedo, exposure or vegetation. Therefore, it is important to establish criteria for considering which characteristic should be preserved in a 'homogeneous unit' of the snow cover area. Obviously, a subdivision of the study area is also subject to the availability of data representative of each partition. Nevertheless, with the same amount and quality of information the developed areal model provides better results than the traditional point location approach.

Acknowledgements

The study of the second author was supported by US EPA (R819658) Center for Ecological Health Research at U.C. Davis.

References

Anderson, E., 1976. A point energy and mass balance model of a snow cover. NOAA Tech. Rep., NWS 19, 150 pp.

Bader, H., Haefeli, R., Bucher, J. et al., 1939. Der Schnee und seine Methamorphose. English Translation 14, Snow and its Metamorphism. Snow, Ice and Permafrost Research Establishment, US ACE, 313 pp.

Businger, J.A., Wyngaard, J.C., Izumi, Y. and Bradley, E.F., 1971. Flux–profile relationships in the atmospheric surface layer. J. Atmos. Sci., 28: 181–189.

DeVries, J. and Franke, C., 1988. Evaporation from snow fields, estimation of potential for control. Final Report for Hatch Project 3055, Water Science and Engineering Paper 3014, University of California, Davis, 88 pp.

Dunne, T., Price, A.G. and Colbeck, S.C., 1976. The generation of runoff from sub-antarctic snowpack. Water Resour. Res., 12(4): 677–685.

Kojima, K., 1967. Densification of seasonal snow cover. In: Physics of Snow and Ice, Proc. Int. Conf. on Low Temperature Science, Vol. 1, Part 2, Hokkaido University, Sapporo, Japan.

Kojima, K. and Motoyama, H., 1985. Melting and heat exchange at the bottom of a snow cover. Ann. Glaciol., 6: 276–277.

Kondo, J. and Yamazaki, T., 1990. A prediction model for snowmelt, snow surface temperature and freezing depth using a heat balance method. J. Appl. Meteorol., 29: 375–384.

Kutchment, L.S., Demidov, V.N. and Motovilov, Y.G., 1983. River Runoff Formation, Physically Based Models. Nauka, Moscow.

Kuz'min, P.P., 1961. Melting of the snow cover. Gidrometeorol. Izd., Leningrad. Translation TT71-55095, Israel Program of Scientific Translation, 1972.

Male, D.H. and Gray, D.M., 1981. Snowcover ablation and runoff. Handbook of Snow, Pergamon Press, New York, pp. 360–436.

Mellor, M., 1964. Some optical properties of snow. IAHS Publ., 69: 128–140.

Mellor, M., 1975. Engineering Properties of Snow. IAHS Publ., 114: 251–291.
Morris, E.M., 1982. Sensitivity of the European Hydrological System snow model. IAHS Publ., 138: 221–231.
Morris, E.M., 1983. Modelling the flows of mass and energy within a snowpack for hydrological forecasting. Ann. Glaciol., 4.
Morris, E.M., 1985. Snow and ice. In: M. Anderson and T.P. Burt (Editors), Hydrological Forecasting, Wiley, Chichester, pp. 154–182.
Motovilov, Y.G., 1986. A model for snow cover formation. IAHS Publ., 155.
Prandtl, L., 1932. Meteorologische Anwendung der Stromungslehre. Beitr. Phys. D, Freien Atmos., 19: 188–202.
Smith, J.L., 1974. Hydrology of warm snowpacks and their effects upon water delivery: some new concepts. In: H.S. Santeford and J.L. Smith (Compilers), Advances in Concepts and Techniques in the Study of Snow and Ice Resources. National Academy of Sciences, Washington, DC, pp. 76–98.
Swinbank, W.C., 1963. A comparison between predictions of dimensionless analysis for the constant-flux layer and observation in unstable conditions. Q. J. R. Meteorol. Soc., 94: 460–467.
Van der Heydt, L., 1991. Application of a point energy balance model of a snow cover. M.S. Dissertation, Dept. of Civil Eng., University of California, Davis.
Williams, L.D., 1972. Application of computed global radiation for areas of high relief. J. Appl. Meteorol., 11: 526–533.
Yen, Y.C., 1962. Effective thermal conductivity of ventilated snow. J. Geophys. Res., 67: 1091–1098.
Yosida, Z., 1955. Physical studies on deposited snow. I. Thermal properties. Contrib. Inst. Low Temp. Sci. Hokkaido, 7: 19–74.